PCCP

RSC Publishing

PAPER

View Article Online
View Journal | View Issue

Cite this: *Phys. Chem. Chem. Phys.*, 2013, **15**, 1509

Structure analysis of substrate catalyst complexes in mixtures with ultrafast two-dimensional infrared spectroscopy†

Andreas T. Messmer,[a] Katharina M. Lippert,[b] Peter R. Schreiner[b] and Jens Bredenbeck*[ac]

The understanding of reaction mechanisms requires structure elucidation of short-lived intermediates, even in the presence of other, similar structures. Here we show that polarization dependent two-dimensional infrared spectroscopy is a powerful method to determine the structure of molecules that participate in fast equilibria, in a regime where standard techniques such as nuclear magnetic resonance spectroscopy are beyond their limits. Using catalyst–substrate complexes in a Lewis acid catalyzed enantioselective Diels–Alder reaction as an example we present two methods that allow the resolution of molecular structure in mixtures even when the spectroscopic signals partially overlap. The structures of *N*-crotonyloxazolidin-2-one, a reactant carrying the Evans auxiliary, and its complex with the Lewis acid $SnCl_4$ were determined in a mixture as used under the typical reaction conditions. In addition to the chelate that mainly forms, three additional substrate–catalyst complexes were detected and could be tentatively assigned. Observation of minor complex conformers suggests a rationale for the observed diastereoselectivity of the reaction using $SnCl_4$ as compared to other Lewis acids. Knowledge about additional species may lead to a better understanding of the different selectivities for various Lewis acids and allow reaction optimization.

Received 16th August 2012,
Accepted 21st November 2012

DOI: 10.1039/c2cp42863f

www.rsc.org/pccp

Introduction

Some of the main challenges in modern chemistry are the development of new catalytic reactions and the optimization of existing ones. This requires a detailed understanding of the underlying reaction mechanisms. Still, many reaction mechanisms are inferred from reactivity and product studies. This is an indirect approach and leaves room for rather broad interpretation. Direct approaches require knowledge about the three dimensional structure of the intermediates present under the reaction conditions. However, these are in most cases short-lived and in (fast) equilibrium with other species. Additionally, they are usually only weakly populated and can hardly be isolated. For these reasons, the intermediate structures are typically not accessible using standard approaches such as multidimensional NMR techniques or crystallographic studies. Methods combining high sensitivity, structural resolution and ultrafast time resolution are required.

In a recent study we showed that polarization-dependent two-dimensional infrared (P2D-IR) spectroscopy is capable of resolving the conformation of small molecules in solution and their complexes with a catalyst.[1] Both, complex formation and dissociation are fast compared to the timescale of NMR. With its inherent (sub)picosecond time resolution and the high sensitivity of infrared spectroscopy, P2D-IR is a powerful technique to investigate the structure of short-lived intermediates. Here we show how the P2D-IR spectra of mixtures can be analyzed and demonstrate that the individual structure of molecules coexisting in equilibria can be determined accurately, even in the case where some infrared bands overlap strongly.

We investigated the catalyst substrate complexes in the Lewis acid catalyzed, enantioselective Diels–Alder reaction (Scheme 1)[2] with the Lewis acid $SnCl_4$. The chiral oxazolidin-2-one moiety,

[a] *Institute of Biophysics, Johann Wolfgang Goethe-University, Max-von-Laue-Str. 1, 60438 Frankfurt, Germany. E-mail: bredenbeck@biophysik.uni-frankfurt.de; Fax: +49 69 794 46421; Tel: +49 69 794 46410*
[b] *Institute of Organic Chemistry, Justus-Liebig University, Heinrich-Buff-Ring 58, 35392 Giessen, Germany. E-mail: prs@org.chemie.uni-giessen.de; Fax: +49 641 99 34309; Tel: +49 641 99 34300*
[c] *CEF-MC, Johann Wolfgang Goethe-University, Max-von-Laue-Str. 9, 60438 Frankfurt, Germany*

† Electronic supplementary information (ESI) available: ^{1}H-NMR and ^{1}H-NOESY spectra, determination of the systematic error, comparison of the computed frequencies with the experiment, additional P2D-IR spectra, computational details. See DOI: 10.1039/c2cp42863f

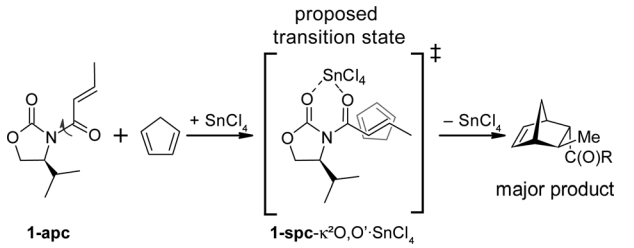

Scheme 1 Top: Enantioselective, Lewis acid catalyzed Diels–Alder reaction of **1** with cyclopentadiene using the Evans auxiliary (R) with the proposed transition state.[2] The conformers of **1** are labeled with their shorthand notation: ap and sp denote the *antiperiplanar* and *synperiplanar* arrangement of the carbonyl group; c and t relate to the s-*cis* and s-*trans* configuration of the C–C single bond.

widely known as the Evans auxiliary, is a common motive used in asymmetric synthesis to impose stereoselectivity.[3,4] The stereochemistry of the reaction is mainly determined by the conformation of *N*-crotonyloxazolidinone (**1**).[2] Using Et_2AlCl as the catalyst, this reaction is a textbook example for dictating the structure of an intermediate through metal chelation.[4,5] Despite the popularity of this approach, the mechanism is mainly derived from the stereochemistry of the product. Only recently, Bakalova *et al.* presented an alternative mechanism based on NMR measurements and DFT computations.[6]

In the study presented here, we analyzed a mixture of free **1** and its $SnCl_4$ complexes and determined the structures of the major complex, chelate **1-spc**-κ^2O,O'·$SnCl_4$, in addition to the structure of the substrate, **1-apc**, under equilibrium conditions. In addition to the primarily formed chelate, three additional complexes formed in low concentration. These were detected and tentatively assigned.

Basics of P2D-IR spectroscopy

A 2D-IR spectrum has two frequency axes; the *y*-axis is called the pump axis, the *x*-axis is the probe axis. In the experiment, the wavelength of a narrowband pump pulse with a duration of ~1.2 ps is scanned across the spectral region of interest. A subsequent broadband probe pulse (~150 fs) measures the absorption change of the sample that is induced by the pump pulse. All spectra shown are therefore plotted as difference spectra. Negative signals are shown in blue, positive signals are shown in red. Analogous to a 2D-NMR spectrum, a typical 2D-IR spectrum of a molecule consists of diagonal peaks and, if the vibrations interact with each other, *i.e.,* couple, cross peaks between them.[7–9] Each peak consists of a negative part, caused by bleach of the ground state absorption and stimulated emission, as well as a red shifted positive part caused by excited state absorption. The signal sizes depend on the size and direction of the transition dipole moments of the involved vibrations and the relative polarization of the pump and probe pulses.[7–12] The dependence on the laser pulse polarization can be quantified by the anisotropy $r(t)$ calculated as

$$r(t) = \frac{\Delta\alpha_{||}(t) - \Delta\alpha_{\perp}(t)}{\Delta\alpha_{||}(t) + 2\Delta\alpha_{\perp}(t)} \quad (1)$$

where $\Delta\alpha_{||}(t)$ and $\Delta\alpha_{\perp}(t)$ are the signal intensities for parallel and perpendicular polarization of the pump and probe pulse.[13–17] For a fixed isotropic distribution of molecules in space, the anisotropy gives direct access to the angle θ between the transition dipole moments of the molecular vibrations *via* the relation

$$\theta = \cos^{-1}\sqrt{\frac{5r(t)+1}{3}} \quad (2)$$

or, alternatively, directly using the signal ratio $\Delta\alpha_{||}(t)/\Delta\alpha_{\perp}(t)$

$$\theta = \cos^{-1}\sqrt{\left(6\frac{\Delta\alpha_{\parallel}(t)}{\Delta\alpha_{\perp}(t)} - 4\right)\Big/\left(3\frac{\Delta\alpha_{\parallel}(t)}{\Delta\alpha_{\perp}(t)} + 3\right)} \quad (3)$$

Because the molecules rotate on the time scale of a 2D-IR measurement, exact values for θ are only obtained if the delay time between the pulses is extrapolated to t = 0 ps.[18]

Material and methods

Experimental

Compound **1** was synthesized following the procedures described in the literature.[2,19] For the P2D-IR measurements it was dissolved in dry dichloromethane (CH_2Cl_2) and mixed with $SnCl_4$.

The P2D-IR setup used is described in detail in ref. 1. The output of a Ti:sapphire-oscillator–amplifier system (Spectra Physics, Spitfire XP, 800 nm, 120 fs, 1 kHz) was used to generate mid-IR pulses (~2.4 μJ per pulse, center frequency around 1660 cm^{-1}, bandwidth ~200 cm^{-1} FWHM, pulse length ~150 fs) in a two-stage optical parametric amplifier.[1,20] In the subsequent pump–probe P2D-IR setup, based on the concept of Hamm *et al.*, the mid-IR pulses were split into a pump, a probe and a reference beam.[21] The pump beam passed a computer controlled Fabry–Perot filter, a chopper running at half the repetition rate of the laser, and was moved in time with respect to the probe pulse using a computer-controlled delay line. The pump and probe beams were focused with an off-axis parabolic mirror in spatial overlap onto the sample cell, which had an optical path length of 250 μm.[22] Special care was taken to obtain proper polarizations of the beams at the sample position. The polarization of the pump beam was rotated by 45° relative to probe and reference beam polarizations.[18,23,24] The polarization contrast at the sample position was >1400 : 1 for the pump and >1200 : 1 for probe and reference. Directly after the sample, the probe and reference beams passed through a motorized, computer controlled polarizer, while the pump beam was blocked. The motorized polarizer swapped every 300 laser pulses between +45° and −45° and therefore allowed the quasi-simultaneous measurement of parallel and perpendicular polarization. After both beams were collimated, they were frequency dispersed by a spectrometer onto a 2 × 32 pixel mercury–cadmium–telluride detector array.

The P2D-IR signal was calculated as the difference in the absorption between the pumped and unpumped sample. The spectra shown in Fig. 1 were measured directly after each other

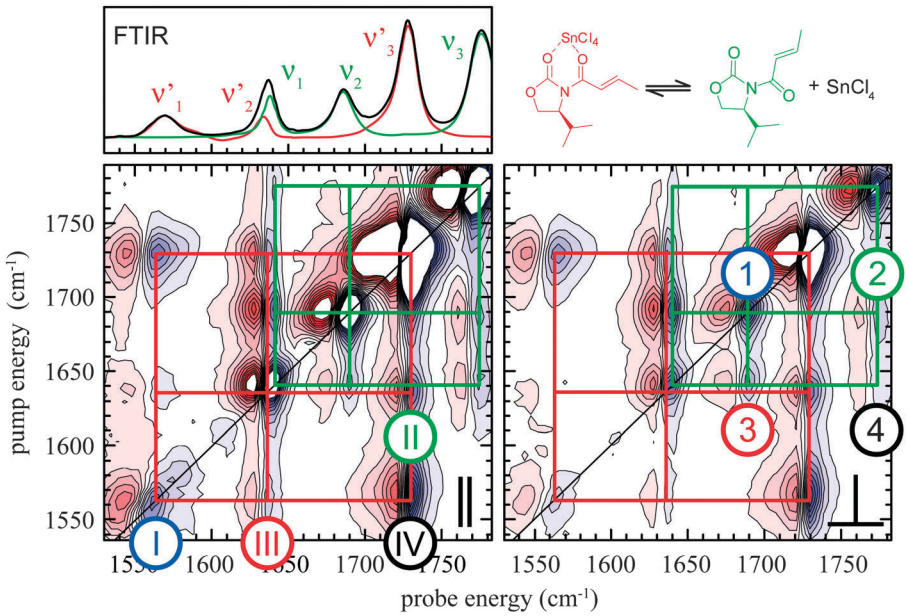

Fig. 1 P2D-IR spectrum for parallel (left) and perpendicular polarization (right) of a mixture of **1** (24 mM) and $SnCl_4$ (24 mM) in CH_2Cl_2 (1.5 ps). The contour lines are spaced by 0.05 mOD. Signals larger than ±0.5 mOD are truncated. The signals that belong to the same species are connected by the grids. Green: free **1**; red: **1**·$SnCl_4$. The FTIR spectra of the mixture (black), **1** (green), and **1**·$SnCl_4$ (red) are shown in the top panel for orientation.

in four blocks to span the entire region of interest, with minimal changes to the setup between measurements. Subsequently, the blocks were set together to form the final spectrum without further treatment.

Quantum chemical computations

All computations were performed by employing the program suite Gaussian 09,[25] using density functional theory (DFT) with Truhlar's hybrid meta-exchange-correlation functional M06[26] in conjunction with a 6-31+G(*d*,*p*) basis set.[1] Computations on Sn-containing species were performed using a 6-31+G(*d*,*p*) basis set with Stuttgart–Dresden effective core potentials (SDD) on the Sn atom.[27] Computations that use a DGDZVP basis set are reported in the ESI.† The influence of the solvent was taken into account by the self-consistent reaction field (SCRF) method, using the polarizable continuum model (PCM)[28] with van der Waals radii of Bondi[29] with the Gaussian 09 default scaling of 1.1 and explicit hydrogen atoms.

Results and discussion

Analysis of the major species present in a mixture of 1 and $SnCl_4$

In previous work we have determined the conformation of **1** to be **1-apc** in solution and the structure of its major $SnCl_4$ complex, the chelate **1-spc**-κ^2O,O'·$SnCl_4$ (see Scheme 1). In both cases, pure solutions of the substances were prepared and analyzed. Fig. 1 shows the P2D-IR spectrum of a 1 : 1 mixture of **1** and $SnCl_4$ in CH_2Cl_2 for parallel (left panel) and perpendicular polarization (right panel). In NMR measurements under such conditions, free **1** and **1**·$SnCl_4$ complexes cannot be detected individually. The exchange between species is faster than the inherent NMR time resolution (ESI†). The rapid exchange does not pose a problem for IR spectroscopy.[30,31] The FTIR spectrum of the mixture is shown in the top panel for orientation (black). It is the sum of the FTIR spectra of free **1**, shown in green, and its Lewis acid complex **1**·$SnCl_4$, shown in red. Both species show three intense bands between 1500 cm^{-1} and 1800 cm^{-1} originating from the carbonyl and alkenyl vibrations of the molecules. The bands of **1** (ν_1, ν_2 and ν_3) shift to lower wavenumber when forming the complex **1**·$SnCl_4$ (ν'_1, ν'_2 and ν'_3). ν_1 and ν'_2 strongly overlap, while all other bands are nicely separated from each other.

The P2D-IR spectrum is also the sum of the P2D-IR spectra of the single species present in solution.[1] The main signals of **1** are connected by the green grid and the ones from **1**·$SnCl_4$ are connected by the red grid. Each signal set consists of nine signals: three diagonal peaks and six cross peaks. The diagonal peaks are most intense in the spectrum measured with the pump and probe polarizations parallel to each other and are approximately three times stronger than those for perpendicular polarization conditions. As mentioned above, the angle between the transition dipole moments of the coupled vibrations can be obtained from the anisotropies of the cross peaks. Because the molecules rotate during the measurement, the anisotropy decays with time and needs to be extrapolated to t = 0 ps to accurately deduce the angle between the transition dipole moments and thus, the three dimensional structure of the molecule. We will refer to this procedure as the *anisotropy method* throughout the paper. The anisotropy time dependence of the peaks marked by numbers in Fig. 1 is shown in Fig. 2 for free **1** (top) and **1**·$SnCl_4$ (bottom). The lines show the linear extrapolations of the measured data points between 1.5 ps and 5 ps (colored crosses). The data points before a delay time of 1.5 ps

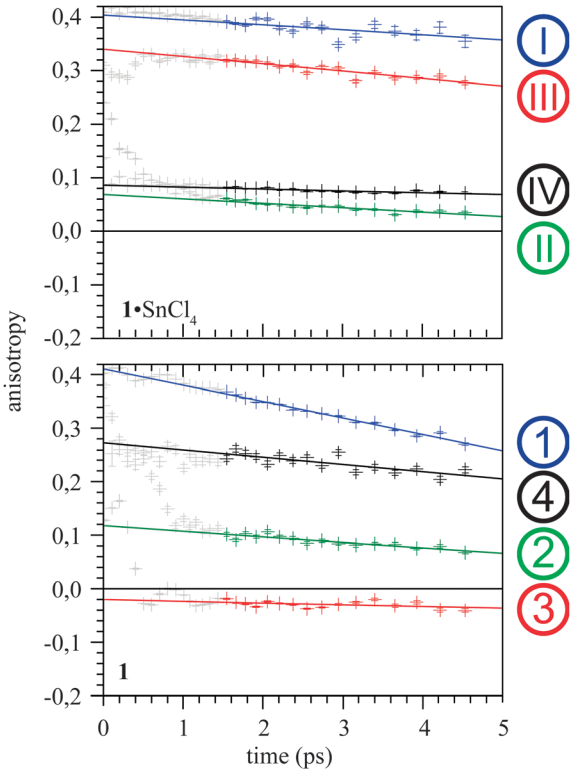

Fig. 2 Time dependence of the anisotropy for the signals marked in Fig. 1. The straight lines show the linear fit of the data from 1.5 ps to 5 ps. Top, diagonal peak ν_2': blue (*cf.* pos. I); cross peak $\nu_2'/\nu_3'/\nu_1'/\nu_2'$: green (*cf.* pos. II); cross peak $\nu_1'/\nu_3'/\nu_2'/\nu_3'$: red (*cf.* pos. III); cross peak $\nu_1'/\nu_2'/\nu_1'/\nu_3'$: black (*cf.* pos. IV). Bottom, diagonal peak ν_2: blue (*cf.* pos. 1); cross peak ν_2/ν_3: green (*cf.* pos. 2); cross peak ν_1/ν_2: red (*cf.* pos. 3); cross peak ν_1/ν_3: black (*cf.* pos. 4).

are not used for analysis because the pump and probe pulse still overlap.

The extrapolation of the diagonal peak I leads to an anisotropy of $r(0) = 0.403(9)$, which agrees very well with the true value of 0.4 that is expected for a 0° transition dipole angle. The anisotropy of cross peak II extrapolates to $r(0) = 0.069(3)$. This translates into an angle of $48° \pm 2°$ between the transition dipole moments of modes ν_2' and ν_3'. The stated error in the angle includes the fit error and estimated experimental errors. The same analysis is performed for all the cross peaks and is summarized in Table 1. All determined angles agree within the experimental error with the ones found by analyzing the pure species in solution.[1]

Table 1 Determined angles between the transition dipole moments for **1** and **1**·$SnCl_4$ in CH_2Cl_2 (anisotropy method)

Cross peak	Modes	Angle θ	Anisotropy $r(0)$
II	ν_1'/ν_2' (°)/ν_1'/ν_3' (°)	$48° \pm 2°$	0.069(3)
III	ν_1'/ν_2'	$18° \pm 4°$	0.340(5)
IV	$\nu_3'/\nu_1'/\nu_2'$	$46° \pm 2°$	0.086(2)
2	ν_2/ν_3	$43° \pm 2°$	0.102(2)
3	ν_1/ν_2	$57° \pm 2°$	−0.020(5)
4	ν_1/ν_3	$27° \pm 3°$	0.273(8)

This shows that it is possible to determine the structure of molecules that are in dynamic equilibrium with each other under conditions where NMR signals are motionally averaged (see ESI†). The overlap of ν_1 and ν_2' in the one-dimensional absorption spectra does not pose a problem, as the cross peaks II and 3 in the two-dimensional spectrum do not overlap.

However, the anisotropy method, in which the anisotropy of the cross peaks is directly evaluated, assumes that the anisotropy is constant over the cross peak and therefore is only applicable if the cross peaks do not overlap significantly. If they do overlap, the measured anisotropy cannot be translated into the individual angles in a straight forward and unique manner. In this case, an alternative approach can be used, in which single cross peaks are selectively annihilated by taking weighted differences in the spectra recorded with parallel and perpendicular polarization ($\Delta\alpha_{||}(t) - x\Delta\alpha_{\perp}(t)$). According to eqn (3) the ratio x of the signals between the spectra measured with parallel and perpendicular polarization also gives direct access to the transition dipole moment angle. In doing so, the band shape of the peaks is also accounted for and thus the single contributions to the signal (*i.e.,* the overlapping peaks) can be identified and analyzed independently. This approach is referred to as the *annihilation method* throughout the paper and is exemplified in Fig. 3 for the mixture of **1** and $SnCl_4$ analyzed above.

The top left spectrum shows the measured P2D-IR spectrum for parallel polarization conditions (*cf.* Fig. 1 left). All other spectra are weighted differences between parallel and perpendicular polarization, where the weighting factor x has been chosen such that the signals at the marked positions are annihilated. The required weighting factors x are shown in the insets and can be translated into the angles between the transition dipole moments. Since we only evaluate one set of spectra with a delay time of 1.5 ps, we cannot extrapolate the ratio to zero delay time. Therefore, the derived angles show a systematic error originating from the rotational diffusion of the molecules within the first 1.5 ps. This error can be estimated based on the anisotropy plots shown in Fig. 2 and is at maximum 3° for the molecules analyzed here and angles larger than 20° (for a detailed discussion see ESI†). The determined angles (see Tables 2 and 3) agree very well with the angles obtained using the anisotropy method. Thus, the annihilation method works well and the two methods are equivalent when the bands do not overlap.

This approach is similar to polarization angle scanning (PAS) 2D-IR spectroscopy introduced by Cho and co-workers.[10,11] In PAS 2D-IR, several 2D-IR spectra are measured in which the polarization conditions between the laser pulses are changed stepwise in order to alter the cross peak intensities. In a simplified picture, this procedure experimentally weights the parallel and perpendicular spectra differently for each measurement. After the measurements, the peak intensities are fitted as a function of the polarization conditions. The conditions where the signals are annihilated give access to the angle between the transition dipole moments. In order to carry out the annihilation based on only two separate measurements for parallel and perpendicular polarization, it is essential that the measurements

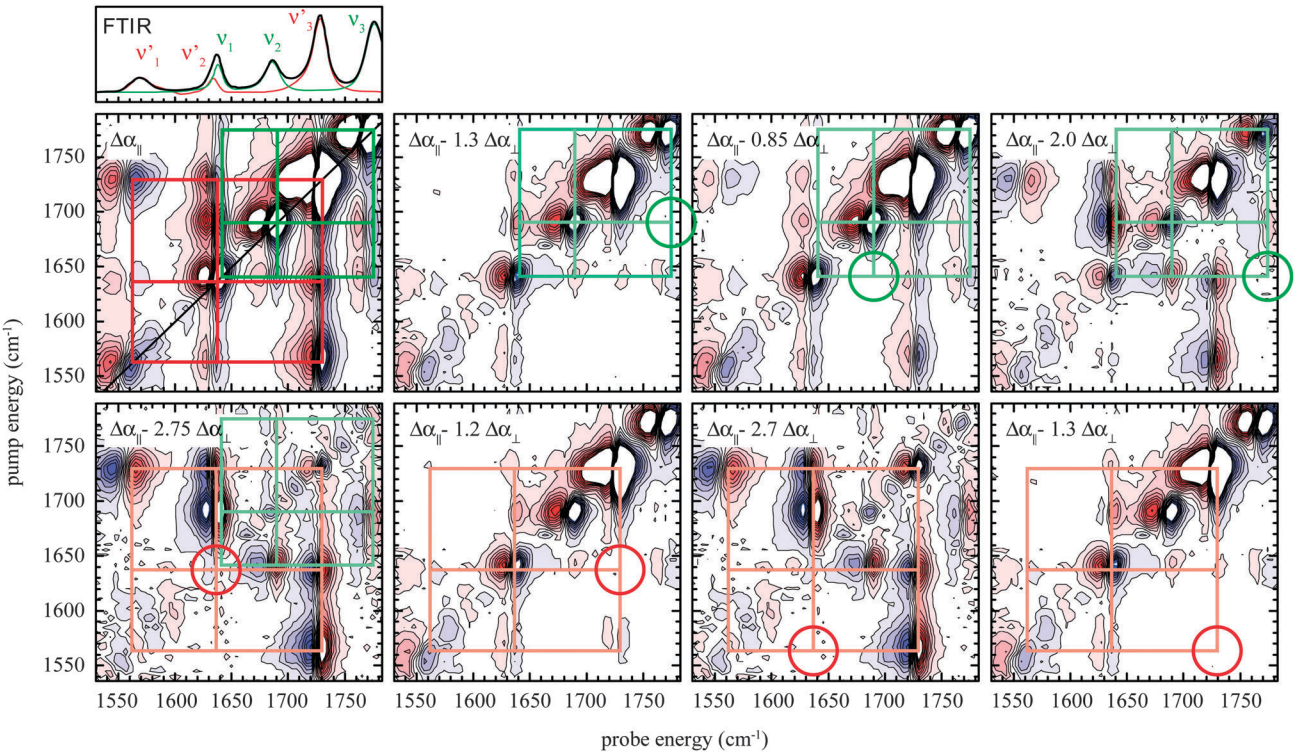

Fig. 3 Differences between the P2D-IR spectra of a mixture of **1** (24 mM) and $SnCl_4$ (24 mM) in CH_2Cl_2 (1.5 ps) measured with parallel and perpendicular polarization. The weighting factors given in the insets are chosen such that the peaks highlighted by the circles are annihilated. The contour lines are spaced by 0.04 mOD. Signals larger than ±0.4 mOD are truncated. The signals that belong to the same species are connected by the grids (green: free **1**; red: **1**·$SnCl_4$).

Table 2 Comparison between the experimentally determined transition dipole moment angles of **1** in CH_2Cl_2 (annihilation method) and the results of DFT computations (M06/6-31+G(*d*,*p*)/PCM/Bondi). The overall deviation of the three angles is expressed as the sum of the single deviations, Δ_{total}

		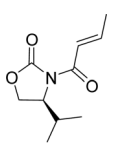	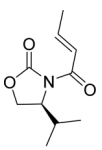	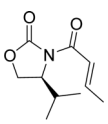	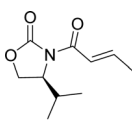
	Experiment at 1.5 ps	**1-apc**	**1-apt**	**1-spt**	**1-spc**
ν_1/ν_2 (°)	60 ± 7	64 (Δ = 4)	33 (Δ = 27)	74 (Δ = 14)	67 (Δ = 7)
ν_1/ν_3 (°)	30 ± 5	21 (Δ = 9)	54 (Δ = 24)	65 (Δ = 35)	42 (Δ = 12)
ν_2/ν_3 (°)	46 ± 2	43 (Δ = 3)	40 (Δ = 6)	52 (Δ = 6)	71 (Δ = 25)
$\Delta_{total} = \Sigma\lvert\Delta_i\rvert$ (°)		16	57	55	44
ΔG_{298} (kcal mol^{-1})		0.0	3.6	6.0	3.3

are carried out under the same conditions, *i.e.,* that the laser power does not change between the measurements. This is accomplished here by a quasi-simultaneous measurement of the spectra with the two different polarization conditions.

Based on the transition dipole angles the molecular structure can be determined. In the ideal case where each stretching vibration is localized on one bond, the angles measured between the transition dipole moments are identical to the angles between the bonds and give direct access to the geometry. However, in most molecules the vibrations are delocalized over several bonds, as is also the case for the systems studied here. In these cases the transition dipole moments of the vibrations are not necessarily aligned parallel to certain bonds. Quantum chemical computations, *e.g.*, based on DFT, provide the orientation of the transition dipole moments in the molecule. In Table 2, the results of the DFT computations for the four conformers of **1** are compared with the experimental values. The experiment agrees very well with the computation for conformer **1-apc**, which is the lowest lying conformer in CH_2Cl_2. There are two possible reasons for the slight deviations between the experiment and theory. First, the computed structure is the energy-minimized structure at 0 K. At room temperature one expects a distribution of structures around the minimal energy structure, leading to small deviations from the expected values. Additionally, the computations are based on the harmonic approximation. This may alter the composition of

Table 3 Comparison between experimentally determined transition dipole moment angles of **1**·$SnCl_4$ in CH_2Cl_2 (annihilation method) and the results of DFT computations (M06/6-31+G(*d*,*p*)/SDD/PCM/Bondi). The overall deviation of the three angles is expressed as the sum of the single deviations, Δ_{total}

	Experiment at 1.5 ps	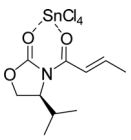 **1-spc**-κ^2O,O'	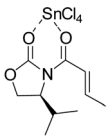 **1-spt**-κ^2O,O'	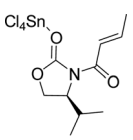 **1-apc**-κO	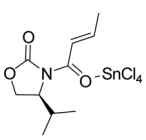 **1-apc**-$\kappa O'$	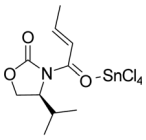 **1-apt**-κO	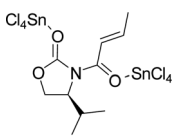 **1-apc**-1κO,2$\kappa O'$
ν_1'/ν_3'	15 ± 8	16 (Δ = 1)	24 (Δ = 9)	56 (Δ = 41)	81 (Δ = 66)	38 (Δ = 23)	84 (Δ = 69)
ν_2'/ν_3'	46 ± 2	46 (Δ = 0)	20 (Δ = 26)	80 (Δ = 34)	20 (Δ = 26)	44 (Δ = 2)	5 (Δ = 41)
ν_2'/ν_3' (°)	49 ± 2	61 (Δ = 12)	42 (Δ = 7)	44 (Δ = 5)	61 (Δ = 12)	38 (Δ = 11)	89 (Δ = 40)
$\Delta_{total} = \Sigma\lvert\Delta_i\rvert$ (°)		13	42	80	104	36	150
ΔG_{298} (kcal mol^{-1})		0.0	6.5	8.4	6.7	10.2	—[a]

[a] The free energy of the di-tin-complex cannot be directly set into relation to the mono-complexes. A comparison of complex dissociation energies is reported in the ESI.

the vibrations and therefore change the orientation of the transition dipole moments compared to the real, anharmonic system. The systematic error caused by rotational diffusion of maximum 3° in the angles determined by the annihilation method is in the range of the experimental errors and has no significant impact (see ESI†). The computed angles and frequencies for the other conformers of **1**, which are higher in free energy, deviate strongly from the values obtained in the experiment. An instructive value for comparison is the sum of the deviations of computed and measured angles. This value is 16° for **1-apc** and higher than 40° for the others. Single angles deviate up to 35° for the angle between ν_1 and ν_2 computed in **1-spt**. This comparison proves that **1-apc** is the conformer present in solution. This is in agreement with the conclusions drawn by the comparison of the computed vibrational energies (see ESI†) and earlier studies on pure solutions of **1**.[1,6,32]

The angles determined by the annihilation method for the complex **1**·$SnCl_4$ match the computations for the chelate **1-spc**-κ^2O,O'·$SnCl_4$ very well (see Table 3). The total deviation between the measurement and the computation is 13°, while it is up to 104° for the other mono-complexes. The di-tin-complex (**1-spc**-1κO,2$\kappa O'$·$(SnCl_4)_2$), also discussed in the literature, is shown in the last entry of Table 3.[6] It deviates even more from the measurement and can be excluded under these conditions. A previous NMR study concluded that a chelate complex is formed, but could not further discriminate between **1-spc**-κ^2O,O'·$SnCl_4$ and **1-spt**-κ^2O,O'·$SnCl_4$.[33] The identification of the chelate **1-spc**-κ^2O,O'·$SnCl_4$ as the major complex formed under these conditions is in agreement with our earlier study.[1] Its percentage of complex population is >80%, the remaining portion is composed of the minor species that are discussed in the following.

Detection of minor species present in mixtures of 1 and $SnCl_4$

Because the method of annihilating distinct cross peaks takes into account the anisotropy of the whole peak, structural inhomogeneities of the sample become accessible. It also allows one to identify overlapping bands more clearly. By analyzing the P2D-IR spectra of the mixtures of **1** and $SnCl_4$ more closely, it is possible to prove the existence of at least three additional complexes in solution. Two of these minor species (A and B) show the same concentration dependence as the major species, while species C is only present at large excess of $SnCl_4$. In NMR experiments, there has been no evidence for these minor complexes (ESI†). A potential cause is the limited sensitivity of NMR spectroscopy. In addition, fast exchange between the various complexes is likely, which makes the detection of minor species present in low concentrations with NMR very difficult or even impossible.

Species A

One minor species becomes apparent in the cross peak between ν_3' and ν_1' (see Fig. 4). The high energy shoulder of the band ν_1' couples to a different part of the band ν_3' (black lines) than the main band (red lines) and shows a slightly different anisotropy, indicating different geometries in the molecule. This is readily seen because the two signals disappear at distinct weighted differences, as illustrated in Fig. 4d and e. The weighting factors where the two parts of the cross peak disappear in Fig. 4 translate into angles of 46° for the major species and 41° for the minor species. Therefore, the angle between these two transition dipole moments needs to be at least 5° smaller than for the major species. Because the bands strongly overlap and the fraction of molecules leading to this cross peak is very small (<15%, estimated by the size of the signal at 1658 cm^{-1}, see ESI†), it is difficult to extract the unperturbed line shape of the minor species and the difference in angle could be larger, but hidden by overlapping effects – even though these are strongly reduced by the annihilation method. The measurement clearly shows that the angle between the transition dipole moment ν_1^A belonging to the high-energy shoulder of ν_1' and the transition dipole moment of ν_3^A is smaller than for the main band. The corresponding cross peak between ν_1' and ν_3' shows the same effect (see Fig. 4b and c). This inhomogeneity shows the same concentration dependence as the major complex **1**·$SnCl_4$ and could not be observed by NMR techniques to date.

The finding of an angle less than 41°, combined with the computed vibrational frequencies, could be interpreted as

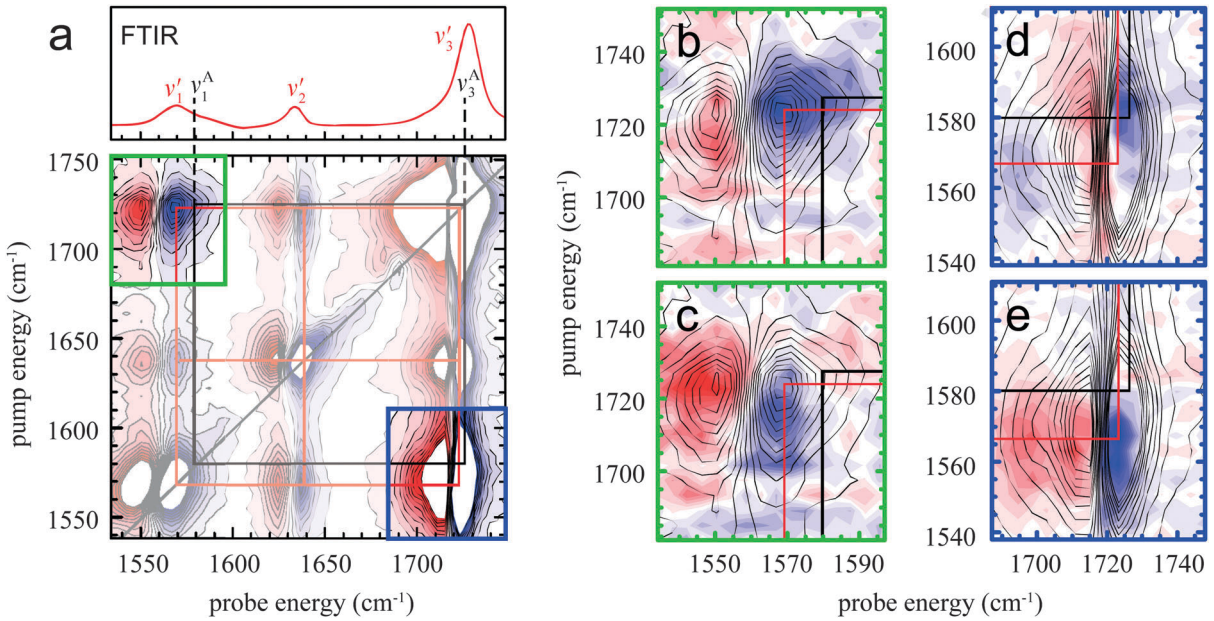

Fig. 4 (a) P2D-IR spectrum (parallel, 1.5 ps) of a solution of **1** (6 mM) and $SnCl_4$ (47 mM) in CH_2Cl_2. The grids indicate the observed coupling pattern (red: major species; black: species A). The contour lines are spaced by 0.04 mOD. Signals larger than ±0.4 mOD are truncated. The FTIR is shown in the top panel. (b–e) Differences between the P2D-IR spectra measured with parallel and perpendicular polarization. Only the regions highlighted (a) are shown. The colored contours are spaced by 6 μOD. The contour lines of the signal in (a) are overlaid for orientation. (b) $\Delta\alpha_{||} - 1.25\Delta\alpha_{\perp}$. (c) $-(\Delta\alpha_{||} - 1.35\Delta\alpha_{\perp})$. (d) $\Delta\alpha_{||} - 1.1\Delta\alpha_{\perp}$. (e) $-(\Delta\alpha_{||} - 1.35\Delta\alpha_{\perp})$.

small amounts of the chelate **1-spt**-κ^2O,O'·$SnCl_4$ in solution (see ESI† for detailed discussion). The presence of conformer **1-spt**-κ^2O,O'·$SnCl_4$ has been hypothesized by Castellino in his NMR study as a potential cause of the low stereoselectivity, however, this claim was without any spectroscopic support.[33]

Species B

A second minor species shows vibrations at ~1570 cm^{-1} (ν_1^B), ~1635 cm^{-1} (ν_2^B) and ~1700 cm^{-1} (ν_3^B). The band ν_3^B appears as a shoulder on the low energy side of band ν_3' and the diagonal peak appears overlapping with the diagonal peak of the major species. This is clearly seen in the slice of the P2D-IR spectrum (Fig. 5a) at 1699 cm^{-1}, which is shown in Fig. 5b (blue). The population of the minor species B can be estimated by comparison with the signal originating from the ^{13}C isotopologue (1.1% natural abundance, Fig. 5b, red curve) to be around 2–4%. The cross peak between ν_1^B and ν_3^B can be seen in the difference between parallel and perpendicular polarization shown in Fig. 5c (highlighted by the black arrow). The angle between the transition dipole moments involved is larger than the angle between ν_1' and ν_3', *i.e.*, larger than 46°. Since the entire peak strongly overlaps with the excited state absorption part of the cross peak between ν_1' and ν_3', the angle cannot be more precisely determined. Additionally, the angle between the transition dipole moments ν_2^B and ν_3^B is larger than that between ν_2' and ν_3', *i.e.,* larger than 49°. The corresponding cross peak is seen in the difference spectrum shown in Fig. 5d (highlighted by the black arrows). The cross peaks of the major species and species B overlap here too, which makes a more precise measurement of the angle unfeasible. The chemical structure of this species could not be derived from the experiment and DFT computations.

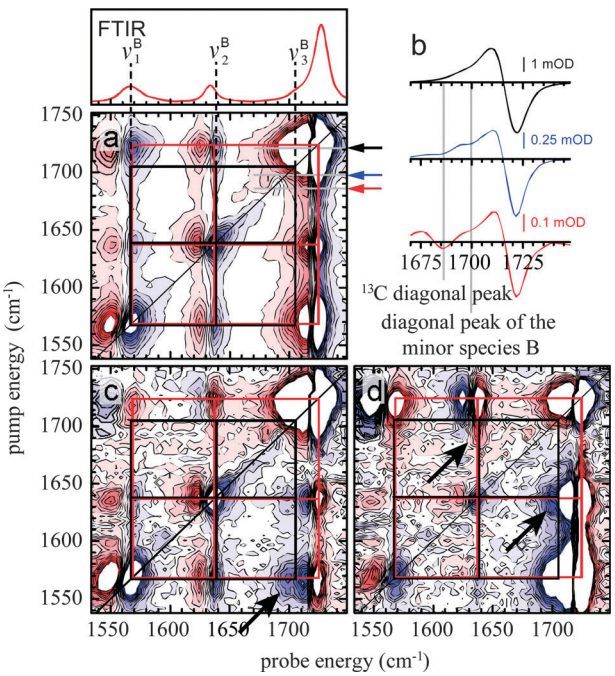

Fig. 5 (a) P2D-IR spectrum (parallel polarization, 1.5 ps) of a mixture of **1** (6 mM) and $SnCl_4$ (47 mM) in CH_2Cl_2. The grids highlight the coupling pattern of the major species (red) and of species B (black). The contour lines are spaced by 0.04 mOD. Signals larger than ±0.4 mOD are truncated. (b) Slices through the spectrum shown in (a) at the marked positions. (c) and (d) Differences between the P2D-IR spectra measured with parallel and perpendicular polarization. The contour lines are spaced by 8 μOD. Signals larger than ±0.09 mOD are truncated. (c) $\Delta\alpha_{||} - 1.5\Delta\alpha_{\perp}$. (d) $\Delta\alpha_{||} - 2.25\Delta\alpha_{\perp}$.

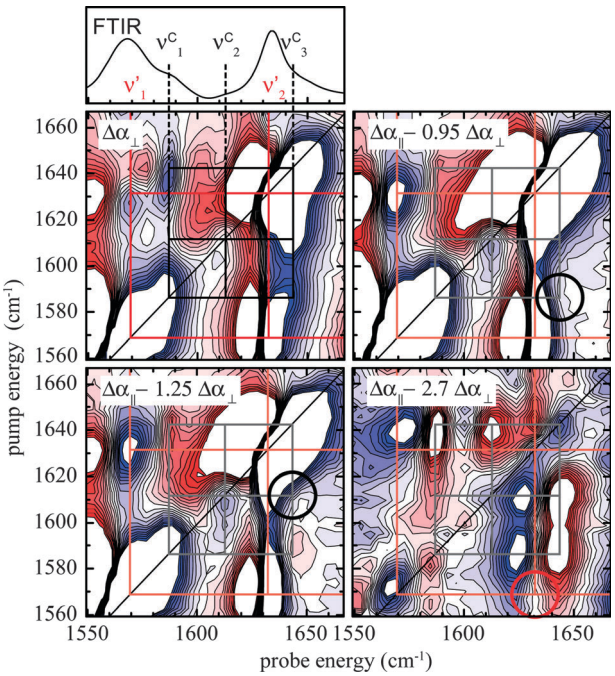

Fig. 6 Differences between the P2D-IR spectra of a mixture of **1** and $SnCl_4$ in CH_2Cl_2 (c_1 = 28 mM; c_{SnCl4} = 531 mM, 1.5 ps). The contour lines are spaced by 9 μOD. Signals larger than ±0.1 mOD are truncated. The signals that belong to the same species are connected by the grids. Red: major complex; black: minor complex. The colored circles highlight the position of the annihilated peaks. The FTIR spectrum of the sample is shown in the top panel for reference.

Species C

In solutions with a large excess of $SnCl_4$, additional vibrations were observed in the FTIR spectra (see Fig. 6 top panel). The coupling between them is highlighted in the 2D-IR spectra with the black grid. Due to strong overlapping effects, only the cross peaks between ν_1^C and ν_3^C and between ν_2^C and ν_3^C are seen. The angles between the corresponding transition dipole moments can be determined by annihilating the cross peaks as 56° ± 8° between ν_1^C and ν_3^C and 50° ± 6° between ν_2^C and ν_3^C (Fig. 6 and ESI†). The angle between ν'_1 and ν'_2 (major species) is found to be 15° ± 4°, which is in perfect agreement with the angle determined earlier (see Table 3). A comparison of the computation for the di-tin-complex **1-spc**-1κO,2$\kappa O'$·$(SnCl_4)_2$ (see Table 3) with the experiment excludes this complex as the source of the signal of species C. In fact, there is no evidence for the formation of **1-spc**-1κO,2$\kappa O'$·$(SnCl_4)_2$ under these conditions, although this structure has been discussed for the Lewis acid Et_2AlCl.[6] The stronger frequency downshift of ν_3 in species C compared to the major species could be caused by the formation a complex between **1** and a $(SnCl_4)_x$ cluster.

Conclusions

We have shown that P2D-IR spectroscopy in combination with quantum chemical computations is able to determine the structure of species coexisting in equilibrium, even under conditions where well-established techniques such as multidimensional NMR spectroscopy fail. The determined angles between the transition dipole moments agree with those determined for the species in a pure solution. Overlapping absorption bands in the FTIR spectrum of a mixture do not pose a difficulty when they are connected to well-separated bands by cross peaks in the P2D-IR spectrum. The annihilation method additionally allows the analysis of congested spectra, where cross peaks overlap and cannot be analyzed using the anisotropy method. Where both methods are applicable, cross validation verifies that the methods agree. A detailed analysis of the P2D-IR spectra of mixtures of **1** and $SnCl_4$ showed that at least four different complexes form in solution at ambient temperature. In addition to the major complex, **1-spc**-$\kappa^2 O,O'$·$SnCl_4$, two more complexes coexist at low concentration of $SnCl_4$. The experimental results in addition to the tentative assignment of the minor species are summarized in Table 4. None of the additional complexes have been observed before and they might be important for understanding the reactivity and selectivity of $SnCl_4$ catalyzed and related reactions. The presence of conformer **1-spt**-$\kappa^2 O,O'$·$SnCl_4$ has, for example, been hypothesized by Castellino as a potential cause of the lower stereoselectivity using $SnCl_4$ compared to other Lewis acids such as Et_2AlCl, however, without direct spectroscopic support. The present study of **1**·$SnCl_4$ complexes highlights the potential of P2D-IR spectroscopy to investigate species that are short-lived or in low concentration in reaction mixtures. This capability makes P2D-IR spectroscopy a powerful tool for future studies of reaction mechanisms.

Table 4 Overview of the detected complexes of **1** and $SnCl_4$ in CH_2Cl_2

	Major species		Species A		Species B		Species C	
Determined structure	**1-spc**-$\kappa^2 O,O'$·$SnCl_4$		Possibly **1-spt**-$\kappa^2 O,O'$·$SnCl_4$		—		Possibly complex with $(SnCl_4)_x$	
Population[a] (%)	>80		<15		2–4		—[b]	
Vibrational band origins (cm^{-1})	ν'_1	1567	ν_1^A	~1575	ν_1^B	~1570	ν_1^C	~1590
	ν'_2	1633			ν_2^B	~1635	ν_2^C	~1610
	ν'_3	1727	ν_3^A	~1730	ν_3^B	~1700	ν_3^C	~1645
Measured angles between the transition dipole moments[c] (°)	ν'_1/ν'_2	15 ± 8						
	ν'_1/ν'_3	46 ± 2	ν_1^A/ν_3^A	<41	ν_1^B/ν_3^B	>46	ν_1^C/ν_3^C	56 ± 8
	ν'_2/ν'_3	49 ± 2			ν_2^B/ν_3^B	>49	ν_2^C/ν_3^C	50 ± 6

[a] At low and moderate $SnCl_4$ concentrations. [b] Only populated at high $SnCl_4$ excess. [c] Measured at a delay time of 1.5 ps.

Acknowledgements

We thank Heike Hausmann (Justus-Liebig University Giessen, Germany) for the NMR measurements. A.T.M. thanks the Fonds der chemischen Industrie (FCI) for a Kekulé fellowship. J.B. thanks the Alexander von Humboldt Foundation for a Sofja Kovalevskaja award.

Notes and references

1 A. T. Messmer, K. M. Lippert, S. Steinwand, E.-B. W. Lerch, K. Hof, D. Ley, D. Gerbig, H. Hausmann, P. R. Schreiner and J. Bredenbeck, *Chem.–Eur. J.*, 2012, **18**, 14989–14995.
2 D. A. Evans, K. T. Chapman and J. Bisaha, *J. Am. Chem. Soc.*, 1988, **110**, 1238–1256.
3 Y. Gnas and F. Glorius, *Synthesis*, 2006, 1899–1930.
4 J. Clayden, N. Greeves, S. Warren and P. Wothers, *Organic chemistry*, Oxford University Press, Oxford, 2001.
5 D. A. Evans, B. D. Allison, M. G. Yang and C. E. Masse, *J. Am. Chem. Soc.*, 2001, **123**, 10840–10852.
6 S. M. Bakalova, F. J. S. Duarte, M. K. Georgieva, E. J. Cabrita and A. G. Santos, *Chem.–Eur. J.*, 2009, **15**, 7665–7677.
7 M. T. Zanni and R. M. Hochstrasser, *Curr. Opin. Struct. Biol.*, 2001, **11**, 516–522.
8 S. Woutersen and P. Hamm, *J. Phys.: Condens. Matter*, 2002, **14**, R1035–R1062.
9 M. Cho, *Chem. Rev.*, 2008, **108**, 1331–1418.
10 J.-H. Choi and M. Cho, *J. Chem. Phys.*, 2010, **133**, 241102.
11 K.-K. Lee, K.-H. Park, S. Park, S.-J. Jeon and M. Cho, *J. Phys. Chem. B*, 2010, **115**, 5456–5464.
12 C. S. Peng, K. C. Jones and A. Tokmakoff, *J. Am. Chem. Soc.*, 2011, **133**, 15650–15660.
13 B. J. Berne and R. Pecora, *Dynamic Light Scattering: With Applications to Chemistry, Biology, and Physics*, Dover Pubn Inc, Dover, 2000.
14 S. S. Andrews, *J. Chem. Educ.*, 2004, **81**, 877–885.
15 O. Golonzka and A. Tokmakoff, *J. Chem. Phys.*, 2001, **115**, 297–309.
16 R. M. Hochstrasser, *Chem. Phys.*, 2001, **266**, 273–284.
17 M. T. Zanni, N.-H. Ge, Y. S. Kim and R. M. Hochstrasser, *Proc. Natl. Acad. Sci. U. S. A.*, 2001, **98**, 11265–11270.
18 Y. L. A. Rezus and H. J. Bakker, *Proc. Natl. Acad. Sci. U. S. A.*, 2006, **103**, 18417–18420.
19 D. Benoit, E. Coulbeck, J. Eames and M. Motevalli, *Tetrahedron: Asymmetry*, 2008, **19**, 1068–1077.
20 P. Hamm, R. A. Kaindl and J. Stenger, *Opt. Lett.*, 2000, **25**, 1798–1800.
21 P. Hamm, M. Lim and R. M. Hochstrasser, *J. Phys. Chem. B*, 1998, **102**, 6123–6138.
22 J. Bredenbeck and P. Hamm, *Rev. Sci. Instrum.*, 2003, **74**, 3188–3189.
23 H. Graener, G. Seifert and A. Laubereau, *Chem. Phys. Lett.*, 1990, **172**, 435–439.
24 K. Ramasesha, S. T. Roberts, R. A. Nicodemus, A. Mandal and A. Tokmakoff, *J. Chem. Phys.*, 2011, **135**, 054509.
25 M. J. Frisch, G. W. Trucks, J. R. Cheeseman, G. Scalmani, M. Caricato, H. P. Hratchian, X. Li, V. Barone, J. Bloino, G. Zheng, T. Vreven, J. A. Montgomery, G. A. Petersson, G. E. Scuseria, H. B. Schlegel, H. Nakatsuji, A. F. Izmaylov, R. L. Martin, J. L. Sonnenberg, J. E. Peralta, J. J. Heyd, E. Brothers, F. Ogliaro, M. Bearpark, M. A. Robb, B. Mennucci, K. N. Kudin, V. N. Staroverov, R. Kobayashi, J. Normand, A. Rendell, R. Gomperts, V. G. Zakrzewski, M. Hada, M. Ehara, K. Toyota, R. Fukuda, J. Hasegawa, M. Ishida, T. Nakajima, Y. Honda, O. Kitao, H. Nakai, T. Vreven, J. A. Montgomery Jr, J. E. Peralta, F. Ogliaro, M. Bearpark, J. J. Heyd, E. Brothers, K. N. Kudin, V. N. Staroverov, R. Kobayashi, J. Normand, K. Raghavachari, A. Rendell, J. C. Burant, S. S. Iyengar, J. Tomasi, M. Cossi, N. Rega, J. M. Millam, M. Klene, J. E. Knox, J. B. Cross, V. Bakken, C. Adamo, J. Jaramillo, R. Gomperts, R. E. Stratmann, O. Yazyev, A. J. Austin, R. Cammi, C. Pomelli, J. W. Ochterski, R. L. Martin, K. Morokuma, V. G. Zakrzewski, G. A. Voth, P. Salvador, J. J. Dannenberg, S. Dapprich, A. D. Daniels, Ö. Farkas, J. B. Foresman, J. V. Ortiz, J. Cioslowski and D. J. Fox, *Gaussian 09 Revision B.01*, Gaussian Inc., Wallingford CT, 2009.
26 Y. Zhao and D. G. Truhlar, *Theor. Chem. Acc.*, 2008, **120**, 215–241.
27 A. Bergner, M. Dolg, W. Küchle, H. Stoll and H. Preuβ, *Mol. Phys.*, 1993, **80**, 1431–1441.
28 J. Tomasi, B. Mennucci and R. Cammi, *Chem. Rev.*, 2005, **105**, 2999–3093.
29 A. Bondi, *J. Phys. Chem.*, 1964, **68**, 441–451.
30 M. C. Thielges and M. D. Fayer, *Acc. Chem. Res.*, 2012, **45**, 1866–1874.
31 Y. S. Kim and R. M. Hochstrasser, *Proc. Natl. Acad. Sci. U. S. A.*, 2005, **102**, 11185–11190.
32 M. Kanai, A. Muraoka, T. Tanaka, M. Sawada, N. Ikota and K. Tomioka, *Tetrahedron Lett.*, 1995, **36**, 9349–9352.
33 S. Castellino, *J. Org. Chem.*, 1990, **55**, 5197–5200.